PERFORMANCE OF HIGH-RESOLUTION TVD SCHEMES FOR 1D DAM-BREAK SIMULATIONS

Gwo-Fong Lin*, Jihn-Sung Lai, and Wen-Dar Guo

ABSTRACT

The performance of high-resolution total variation diminishing (TVD) schemes for simulating dam-break problems are presented and evaluated. Three robust and reliable first-order upwind schemes, namely FVS, Roe and HLLE schemes, are extended to six second-order TVD schemes using two different approaches, the Sweby flux limiter approach and the direct MUSCL-Hancock slope limiter. For idealized dam-break flows, comparisons of the simulated results with the exact solutions show that the flux vector splitting (FVS) scheme coupled with the direct MUSCL-Hancock (DMH) slope limiter approach has the best numerical performance among the presented schemes. Application of the FVS-DMH scheme to a dam-break experiment with sloping dry bed shows that the simulated water depths agree well with the measured.

Key Words: high-resolution total variation diminishing (TVD) scheme, dam-break problem, flux vector splitting (FVS), direct MUSCL-Hancock (DMH) slope limiter approach.

I. INTRODUCTION

Since the Saint Venant equations for 1D dam-break flows are a hyperbolic system of partial differential equations, they may generate a shock in the solution. In general, two approaches to obtaining the solutions containing discontinuities are available: the shock-fitting approach and the shock-capturing approach (LeVeque, 1992; Toro, 2001). In the shock-fitting approach, discontinuities are fitted and computed as true discontinuities (LeVeque, 1992). On the other hand, the shock-capturing approach has the ability to automatically produce correct approximations to discontinuous solutions, without explicit tracking or use of jump conditions (LeVeque, 1992).

Over the past decade, a great deal of progress has been made in the development of so-called high-resolution total variation diminishing (TVD) schemes for hyperbolic conservation laws (Hirsch, 1990; Tan, 1992; Toro, 1997). The high-resolution TVD schemes, belonging to the shock-capturing approach, resolve sharp discontinuities without spurious oscillations in the vicinity of large gradients and do not produce too much numerical dissipation. In developing a high-resolution TVD scheme, a first-order upwind scheme is commonly used as a basis. Basically, the first-order upwind schemes can be categorized into two classes: the flux-difference splitting (FDS) scheme and the flux-vector splitting (FVS) scheme (Hirsch, 1990).

Recently, these high-resolution TVD schemes have been widely employed to solve dam-break problems (Alcrudo *et al.*, 1992; Garcia-Navarro *et al.*, 1992; Yang *et al.*, 1993; Jha et al., 1995; Zhao *et al.*, 1996; Delis and Skeels, 1998; Delis *et al.*, 2000; Tseng and Chu, 2000; Zoppou and Roberts, 2003; Delis, 2003). Among TVD schemes reviewed, the FDS-type schemes (the Roe and HLLE schemes) and their second-order extensions are most commonly employed and evaluated. However, the FVS scheme and its different second-order extensions are rarely applied in dam-break problems. Basically, the FVS scheme is more efficient than the FDS scheme (Toro, 1997). The authors (Lin *et al.*, 2003) proposed and

*Corresponding author. (Tel: 886-2-23676408; Fax: 886-2-23631558; Email: gflin@ntu.edu.tw)

G. F. Lin is with the Department of Civil Engineering, National Taiwan University, Taipei, Taiwan 106, R.O.C.

J. S. Lai and W. D. Guo are with the Hydrotech Research Institute, National Taiwan University, Taipei, Taiwan 106, R.O.C.

compared four second-order FVS-type schemes, including the Liou-Steffen, van Leer, Steger-Warming, and local Lax-Friedrichs schemes. We found that the Liou-Steffen FVS scheme is the most accurate among the four schemes tested, and it avoids an entropy-violating solution without any additional problems. Therefore, the Liou-Steffen FVS scheme is selected to compare with the Roe and HLLE schemes in the present study.

In this paper, three types of schemes are comprehensively evaluated: upwind schemes that are first-order-accurate, flux-limited schemes that are second-order-accurate, and slope-limited schemes that are second-order-accurate. Herein, first-order upwind schemes evaluated include the FVS, Roe and HLLE schemes. Flux-limited schemes based on Sweby's flux limiter approach include the FVS-Sweby, Roe-Sweby and HLLE-Sweby schemes. Slope-limited schemes based on the direct MUSCL-Hancock slope limiter approach include the FVS-DMH, Roe-DMH and HLLE-DMH schemes. The entropy corrections are incorporated in the Roe scheme, while the FVS and HLLE schemes do not require corrections. The simulated solutions solved by three first-order schemes and six second-order schemes are compared with exact solutions for idealized dam-break flows to evaluate the numerical accuracy and computational efficiency. The comparisons of simulated solutions with the experimental data in the case of sudden dam collapse are also presented to demonstrate the applicability of the presented scheme.

II. GOVERNING EQUATIONS

Based on the assumption of hydrostatic-pressure distribution, incompressibility of water and gentle bottom slope of the channel, the 1D dam-break unsteady flows in a rectangular channel can be described mathematically by the Saint Venant equations. Under the Saint Venant hypotheses, 1D unsteady flow can be expressed in conservation form as follows:

$$\frac{\partial \boldsymbol{U}}{\partial t} + \frac{\partial \boldsymbol{F}}{\partial x} = \boldsymbol{S} \tag{1}$$

in which

$$\boldsymbol{U} = \begin{bmatrix} h \\ hu \end{bmatrix};\ \boldsymbol{F} = \begin{bmatrix} hu \\ hu^2 + \frac{1}{2}gh^2 \end{bmatrix};\ \boldsymbol{S} = \begin{bmatrix} 0 \\ gh(s_0 - s_f) \end{bmatrix} \tag{2}$$

where $\boldsymbol{U}$ is the vector of conserved variables; $\boldsymbol{F}$ is the flux vectors in the x-direction; $\boldsymbol{S}$ is the vector of the source terms; t refers to time; x is the horizontal distance along a channel; h is the water depth; u is the depth-averaged velocity; g is the gravity acceleration; s_0 is the slope of the channel bottom; and s_f is the friction slope that can be estimated by the Manning formula.

Using the chain rule gives the quasi-linear form of Eq. (1):

$$\frac{\partial \boldsymbol{U}}{\partial t} + \boldsymbol{A}(\boldsymbol{U})\frac{\partial \boldsymbol{U}}{\partial x} = 0 \tag{3}$$

where $\boldsymbol{A}$ is the Jacobian matrix of $\boldsymbol{F}$. It is defined by:

$$\boldsymbol{A} = \frac{\partial \boldsymbol{F}}{\partial \boldsymbol{U}} = \begin{bmatrix} 0 & 1 \\ c^2 - u^2 & 2u \end{bmatrix} \tag{4}$$

where $c = \sqrt{gh}$ is the celerity of the gravity wave. The Jacobian matrix $\boldsymbol{A}$ has a set of independent and real eigenvalues, λ_k, (k = 1, 2), which are

$$\lambda_1 = u + c;\ \lambda_2 = u - c \tag{5}$$

The independent and real eigenvectors $\boldsymbol{R}^{(k)}$, (k = 1, 2) of the matrix $\boldsymbol{A}$ are expressed as:

$$\boldsymbol{R}^1 = [1,\ u + c]^T;\ \boldsymbol{R}^2 = [1,\ u - c]^T \tag{6}$$

III. NUMERICAL SCHEMES

1. First-Order Upwind Schemes

The Saint Venant equations are a hyperbolic partial differential system, which involve discontinuous as well as smooth solutions. To compute the discontinuities accurately, a conservative numerical scheme must be used (LeVeque, 1992). However, the conservative numerical schemes are only appropriate for solving the homogenous part of Eq. (1). To deal with the source terms, the fractional splitting technique (Toro, 2001) is employed herein. The splitting can be expressed as:

$$\boldsymbol{U}^{n+1} = O^{(\Delta t)} H^{(\Delta t)}(\boldsymbol{U}^n) \tag{7}$$

in which $H^{(\Delta t)}$ is the homogeneous solution operator, $O^{(\Delta t)}$ is the ordinary differential equation operator, n is the time level, and Δt is the time increment. Based on Eq. (7), a general form of first-order explicit conservative schemes for Eq. (1) is given by:

$$\overline{\boldsymbol{U}}_i^{n+1} = \boldsymbol{U}_i^n - \tau(\boldsymbol{F}_{i+1/2}^{(1)} - \boldsymbol{F}_{i-1/2}^{(1)})^n \tag{8}$$

$$\boldsymbol{U}_i^{n+1} = \overline{\boldsymbol{U}}_i^{n+1} + \Delta t \boldsymbol{S}[(\boldsymbol{U}_i^n + \overline{\boldsymbol{U}}_i^{n+1})/2] \tag{9}$$

where τ (= $\Delta t/\Delta x$) is the mesh ratio with the grid size Δx and time increment Δt, and $\boldsymbol{F}_{i+1/2}^{(1)}$ is the first-order intercell numerical flux, which approximates the time-averaged flux across the cell interface at $x = x_{i+1/2}$ between cells i and $i + 1$, where a cell is given

by the spatial interval between $x_{i-1/2}$ and $x_{i+1/2}$. In the present study, three first-order upwind schemes, including the Liou-Steffen FVS, Roe FDS, and HLLE FDS schemes, are employed to obtain the numerical flux $\boldsymbol{F}^{(1)}_{i+1/2}$. Their corresponding numerical flux functions $\boldsymbol{F}_{i+1/2}(\boldsymbol{U}_i, \boldsymbol{U}_{i+1})$ are briefly described below.

(i) Flux Vector Splitting (FVS) Scheme

The flux vector splitting (FVS) scheme described here was originally proposed by Liou and Steffen (1993) for the solution of the Euler equations. Following the development of Liou and Steffen (1993), the flux vector $\boldsymbol{F}(\boldsymbol{U})$ can be decomposed into a convective component $\boldsymbol{F}_C$ and a pressure component $\boldsymbol{P}$ as

$$\boldsymbol{F} = \begin{bmatrix} hu \\ hu^2 + \dfrac{gh^2}{2} \end{bmatrix} = \begin{bmatrix} hu \\ hu^2 \end{bmatrix} + \begin{bmatrix} 0 \\ p \end{bmatrix} = \boldsymbol{F}_C + \boldsymbol{P} \tag{10}$$

where $p = gh^2/2$ is the hydrostatic pressure. Then introducing the Froude number ($F_r = u/c$) into the convective flux vector, one obtains

$$\boldsymbol{F}_C = F_r \boldsymbol{\Phi} = F_r \begin{bmatrix} hc \\ huc \end{bmatrix} \tag{11}$$

Based on the van Leer flux-splitting technique, the first-order numerical flux function is expressed as

$$\boldsymbol{F}^{FVS}_{i+1/2}(\boldsymbol{U}_i, U_{i+1}) = \mathcal{F}^{+}_r(F_r)_i \boldsymbol{\Phi}_i + \mathcal{P}^{+}(F_r)_i \boldsymbol{P}_i + \mathcal{F}^{-}_r(F_r)_{i+1} \boldsymbol{\Phi}_{i+1} + \mathcal{P}^{-}(F_r)_{i+1} \boldsymbol{P}_{i+1} \tag{12}$$

where $\mathcal{F}^{\pm}_r$ and $\mathcal{P}^{\pm}$ are respectively the split Froude number and pressure functions, which can be expressed as (Lin *et al.*, 2003):

$$\mathcal{F}^{\pm}_r(F_r) = \begin{cases} \pm \dfrac{1}{4}(F_r \pm 1)^2 & \text{if } |F_r| \le 1 \\ \dfrac{1}{2}(F_r \pm |F_r|) & \text{otherwise} \end{cases} \tag{13}$$

and

$$\mathcal{P}^{\pm}(F_r) = \begin{cases} \dfrac{1}{4}(F_r \pm 1)^2(2 \mp F_r) & \text{if } |F_r| \le 1 \\ \dfrac{1}{2F_r}(F_r \pm |F_r|) & \text{otherwise} \end{cases} \tag{14}$$

The general form of Eqs. (8) and (9) using the presented FVS numerical flux function is referred to as the FVS scheme herein.

(ii) Roe Scheme

The Roe scheme is devised based on the linearized form of Eq. (1). Roe's numerical flux function is (Roe, 1981)

$$\boldsymbol{F}^{\text{Roe}}_{i+1/2}(\boldsymbol{U}_i, \boldsymbol{U}_{i+1}) = \frac{1}{2}[\boldsymbol{F}(\boldsymbol{U}_i) + \boldsymbol{F}(\boldsymbol{U}_{i+1})] - \frac{1}{2}\sum_{k=1}^{2} \tilde{\alpha}_k |\tilde{\lambda}_k| \tilde{\boldsymbol{R}}^k \tag{15}$$

where $\tilde{\lambda}_k$, $\tilde{\alpha}_k$ and $\tilde{\boldsymbol{R}}^k$ are respectively the average approximate eigenvalues, wave strengths, and eigenvectors. They can be expressed as follows:

$$\tilde{\lambda}_1 = \tilde{u} - \tilde{c}\,, \quad \tilde{\lambda}_2 = \tilde{u} + \tilde{c} \tag{16}$$

$$\tilde{\alpha}_1 = \frac{1}{2}[\Delta h - \frac{\tilde{h}}{\tilde{c}}\Delta u]\,, \quad \tilde{\alpha}_2 = \frac{1}{2}[\Delta h - \frac{\tilde{h}}{\tilde{c}}\Delta u] \tag{17}$$

$$\tilde{\boldsymbol{R}}^1 = [1, \tilde{u} + \tilde{c}]^T\,; \quad \tilde{\boldsymbol{R}}^2 = [1, \tilde{u} - \tilde{c}]^T \tag{18}$$

with

$$\Delta h = h_{i+1} - h_i,\ \Delta u = u_{i+1} - u_i \tag{19}$$

in which $\tilde{u}$, $\tilde{c}$, and $\tilde{h}$ are called the Roe average. They can be obtained from:

$$\tilde{u} = \frac{\sqrt{h_i}u_i + \sqrt{h_{i+1}}u_{i+1}}{\sqrt{h_i} + \sqrt{h_{i+1}}}\,; \quad \tilde{c} = \sqrt{\frac{g(h_i + h_{i+1})}{2}}\,; \quad \tilde{h} = \sqrt{h_i h_{i+1}} \tag{20}$$

For practical computations, the Roe scheme requires an entropy fix to avoid nonphysical solutions. In this paper, the implementation of the entropy correction given by Harten and Hyman (1983) is employed. Hence, the average approximate eigenvalues $|\tilde{\lambda}_k|$ in Eq. (15) are modified as $|\tilde{\lambda}_k|_{\text{mod}}$

$$|\tilde{\lambda}_k|_{\text{mod}} = \max[|\tilde{\lambda}_k|,\ \max(0, \tilde{\lambda}_k - \lambda_i, \lambda_{i+1} - \tilde{\lambda}_k)] \tag{21}$$

Using the above formula, the entropy correction is enforced only when an entropy violating discontinuity appears. The general form of Eqs. (8) and (9) using the presented Roe FDS numerical flux function is referred to as the Roe scheme herein.

(iii) HLLE Scheme

Harten *et al.* (1983) proposed the HLL scheme, which can avoid entropy-violating solutions. Based on their work, Einfeldt (1988) introduced the Roe averages into the HLL scheme for improving the numerical accuracy. The resulting scheme is called the HLLE scheme. The HLLE numerical flux function can be written as:

$$\boldsymbol{F}^{\mathrm{HLLE}}_{i+1/2}(\boldsymbol{U}_i, \boldsymbol{U}_{i+1})$$

$$= \frac{1}{2}[\boldsymbol{F}(\boldsymbol{U}_i) + \boldsymbol{F}(\boldsymbol{U}_{i+1})] - \frac{1}{2}\sum_{k=1}^{2} \tilde{\alpha}_k |\tilde{q}_k| \tilde{\boldsymbol{R}}^k \qquad (22)$$

with

$$\tilde{q}_k = \frac{b^+ + b^-}{b^+ - b^-}\tilde{\lambda}_k - 2\frac{b^+ b^-}{b^+ - b^-} \qquad (23)$$

where $\tilde{\lambda}_k$ and the eigenvalues described in the previous section for the Roe linearizations, and b^+ and b^- are presented as:

$$b^+ = \max(b^R, 0);\ b^- = \max(b^L, 0) \qquad (24)$$

where b^R and b^L are numerical approximations for the maximum and minimum characteristic speeds at the respective locations. They are defined as

$$b^R = \max(u_{i+1} + c_{i+1},\ \tilde{\lambda}_1);\ b^L = \min(u_i - c_i,\ \tilde{\lambda}_2) \qquad (25)$$

where $\tilde{\lambda}_1 = \tilde{u} + \tilde{c}$ and $\tilde{\lambda}_2 = \tilde{u} - \tilde{c}$ are taken as the same as Roe's average eigenvalues in Eq. (16). Using the presented HLLE FDS numerical flux function, the general form of Eqs. (8) and (9) is denoted as the HLLE scheme herein.

2. Second-Order Extensions

Harten (1983) derived a sufficient set of TVD conditions and constructed a modified-flux TVD scheme; since then, a variety of second-order TVD schemes have been developed (Sweby, 1984; Yee, 1987; Toro, 2001). Most of the TVD schemes essentially are constructed with an idea limiter incorporated in the second-order schemes to damp out oscillations. To provide a second-order accuracy including the source terms, a general form of the second-order TVD schemes for Eq. (1) can be written as (Strang, 1968)

$$\boldsymbol{U}^{n+1} = O^{(\Delta t/2)} H^{(\Delta t)} O^{(\Delta t/2)}(\boldsymbol{U}^n) \qquad (26)$$

where

$$H^{(\Delta t)}(\boldsymbol{U}_i^n) \equiv \boldsymbol{U}_i^n - \tau(\boldsymbol{F}^{(2)}_{i+1/2} - \boldsymbol{F}^{(2)}_{i-1/2})^n \qquad (27)$$

$$O^{(\Delta t)}(\boldsymbol{U}_i^n) \equiv \boldsymbol{U}_i^n + \Delta t \boldsymbol{S}_i^n + \frac{\Delta t^2}{2}\left(\frac{\partial \boldsymbol{S}}{\partial \boldsymbol{U}}\right)_i^n \boldsymbol{S}_i^n \qquad (28)$$

in which $\boldsymbol{F}^{(2)}_{i+1/2}$ is the second-order numerical flux. In the present study, the Sweby flux-limiter approach and the direct MUSCL-Hancock slope limiter approach are adopted to obtain the second-order numerical flux.

(i) Sweby's Flux-Limiter Approach

Sweby (1984) developed the technique of obtaining a second-order TVD scheme by adding the antidiffusive flux with a limiter to a first-order scheme. In the present study, high-resolution TVD schemes based on first-order upwind schemes described previously by adding a limited antidiffusive flux are applied to solve the Saint Vennat equations.

By splitting the flux at a cell interface, the flux difference is defined as:

$$(\Delta \boldsymbol{F}_{i+1/2})^+ = \boldsymbol{F}_{i+1} - \boldsymbol{F}^{(1)}_{i+1/2};\ (\Delta \boldsymbol{F}_{i+1/2})^- = \boldsymbol{F}^{(1)}_{i+1/2} - \boldsymbol{F}_i \qquad (29)$$

and note that

$$(\Delta \boldsymbol{F}_{i+1/2})^+ + (\Delta \boldsymbol{F}_{i+1/2})^- = \Delta \boldsymbol{F}_{i+1/2} = \boldsymbol{F}_{i+1} - \boldsymbol{F}_i \qquad (30)$$

such that

$$(\Delta \boldsymbol{F}_{i+1/2})^- + (\Delta \boldsymbol{F}_{i-1/2})^+ = \boldsymbol{F}^{(1)}_{i+1/2} - \boldsymbol{F}^{(1)}_{i-1/2} \qquad (31)$$

Then adding both limited positive and negative fluxes to a first-order numerical flux $\boldsymbol{F}^{(1)}_{i+1/2}$, one obtains a second-order numerical flux $\boldsymbol{F}^{(2)}_{i+1/2}$:

$$\boldsymbol{F}^{(2)}_{i+1/2} = \boldsymbol{F}^{(1)}_{i+1/2} + [\phi(r_i^+)\alpha^+_{i+1/2}(\Delta \boldsymbol{F}_{i+1/2})^+ - \phi(r^-_{i+1})\alpha^-_{i+1/2}(\Delta \boldsymbol{F}_{i+1/2})^-] \qquad (32)$$

where

$$r_i^+ = \frac{\alpha^+_{i-1/2}(\Delta \boldsymbol{F}_{i-1/2})^+}{\alpha^+_{i+1/2}(\Delta \boldsymbol{F}_{i+1/2})^+};\ r^-_{i+1} = \frac{\alpha^-_{i+3/2}(\Delta \boldsymbol{F}_{i+3/2})^-}{\alpha^-_{i+1/2}(\Delta \boldsymbol{F}_{i+1/2})^-} \qquad (33)$$

$$\alpha^+_{i+1/2} = \frac{1}{2}\left(1 - \tau\frac{(\Delta \boldsymbol{F}_{i+1/2})^+}{\Delta \boldsymbol{U}_{i+1/2}}\right);$$

$$\alpha^-_{i+1/2} = \frac{1}{2}\left(1 + \tau\frac{(\Delta \boldsymbol{F}_{i+1/2})^-}{\Delta \boldsymbol{U}_{i+1/2}}\right) \qquad (34)$$

$$\Delta \boldsymbol{U}_{i+1/2} = \boldsymbol{U}_{i+1} - \boldsymbol{U}_i \qquad (35)$$

where ϕ is called the non-linear flux limiter which plays an important role in obtaining monotonic solutions. Several forms of flux limiter have been proposed (Hirsch, 1990). In the present study, the van Leer limiter is applied to ensure the TVD property and it is expressed as:

$$\phi(r) = \frac{r + |r|}{1 + |r|} \qquad (36)$$

Any of the upwind numerical flux function presented in Section III.1 can be applied in this flux-limiter approach. For convenience, the second-order extensions of the FVS, Roe, and HLLE scheme using Sweby's flux limiter approach are referred to as the FVS-Sweby, Roe-Sweby and HLLE-Sweby schemes, respectively.

(ii) Direct MUSCL-Hancock Slope Limiter Approach

The original MUSCL-Hancock approach proposed by van Leer (1984) is a two-step approach, which can be a second-order extension of the Godunov-type upwind scheme. This approach can be applied to the system of non-linear hyperbolic conservation laws, for example, the Saint Vennet equations. The original MUSCL-Hancock slope limiter approach can achieve second-order accuracy in space and time by reconstructing the solution via piecewise linear functions, evolving boundary-extrapolated values in time, and solving a conventional piecewise constant Riemann problem.

In the present study, a more direct method proposed by Toro (2001) is adopted to avoid the decoding of variables in the original two-step MUSCL-Hancock slope limiter approach by formulating the equations in terms of a vector $\boldsymbol{W}$ of flow variables. Therefore, the two-step approach can be reduced to the direct MUSCL-Hancock slope limiter approach, which is a single step method. Since there are fewer computational steps in the direct MUSCL-Hancock slope limiter approach, the computational time should be less the time used by the original two-step MUSCL-Hancock slope limiter approach.

According to the MUSCL method (van Leer, 1979), the left and right data at the interface $x = x_{i+1/2}$, $\boldsymbol{U}_i$ and $\boldsymbol{U}_{i+1}$, are reconstructed as

$$\boldsymbol{U}_i \equiv \boldsymbol{W}_i + \frac{1}{2}[\boldsymbol{I} - \frac{\Delta t}{\Delta x}\boldsymbol{M}(\boldsymbol{W}_i)]\overline{\Delta}_i \tag{37}$$

$$\boldsymbol{U}_{i+1} \equiv \boldsymbol{W}_{i+1} + \frac{1}{2}[\boldsymbol{I} - \frac{\Delta t}{\Delta x}\boldsymbol{M}(\boldsymbol{W}_{i+1})]\overline{\Delta}_{i+1} \tag{38}$$

where $\boldsymbol{W} = [h, u]^T$ is the flow variable vector for the Saint Venant equations, $\boldsymbol{W}_i$ is the cell average data, $\boldsymbol{I}$ is the identity matrix, $\overline{\Delta}_i$ is a slope limiter, and matrix $\boldsymbol{M}(\boldsymbol{W}) = \partial \boldsymbol{F}/\partial \boldsymbol{W}$ can be expressed as

$$\boldsymbol{M} = \begin{bmatrix} u & h \\ g & u \end{bmatrix} \tag{39}$$

In the present study, the van Leer limiter is employed and expressed as

$$\overline{\Delta}_i = [\mathrm{sgn}(\Delta_{i+1/2}) + \mathrm{sgn}(\Delta_{i-1/2})]\frac{|\Delta_{i+1/2}| \cdot |\Delta_{i-1/2}|}{|\Delta_{i+1/2}| + |\Delta_{i-1/2}|} \tag{40}$$

where $\Delta_{i-1/2} = \boldsymbol{W}_i - \boldsymbol{W}_{i-1}$, $\Delta_{i+1/2} = \boldsymbol{W}_{i+1} - \boldsymbol{W}_i$ and sgn refers to the sign-function (Hirsch, 1990).

Therefore, the second-order numerical flux with monotonicity conditions in Eq. (27) can be obtained from the restricted cell-interface variables expressed in Eqs (37) and (38). Then using any of the first-order numerical flux functions presented in Section III.1, one obtains the second-order numerical flux. For convenience, the second-order extensions of the FVS, Roe, and HLLE schemes using direct MUSCL-Hancock slope limiter approach are referred to as the FVS-DMH, Roe-DMH, and HLLE-DMH schemes, respectively.

3. Stability and Boundary Conditions

A characteristic feature of explicit difference schemes is the limits on the time step Δt, which is governed by the stability criteria. In order to ensure numerical stability, the time step is restricted by a well-known Courant-Friedrich-Lewy (CFL) stability condition (Chaudhry, 1993), which can be written as

$$\Delta t = C_n \frac{\Delta x}{\max(|u| + \sqrt{gh})} \tag{41}$$

where C_n is the Courant number (≤ 1), and Δx is the grid spacing. With known grid spacing and flow conditions, the time step is evaluated using Eq. (41).

The boundary conditions used herein are divided into two different types: the land boundary and the open boundary (Zhao *et al.*, 1996). For the land boundary, the velocity normal to the land is set to zero to represent no flux through the boundary. At the open boundary, it is necessary to solve a boundary Riemann problem (Zhao *et al.*, 1996).

IV. DAM-BREAK SIMULATIONS

1. Idealized Dam-Break Flows

In this section, the performance of the first-order and second-order schemes is tested by idealized one-dimensional dam-break flow problems. The schematic diagram of the dam-break flow in a rectangular, frictionless, and horizontal channel is shown in Fig. 1, where h_d and h_u are initial water depths at the downstream and upstream of the dam, respectively. At time $t = 0^+$, the dam is removed instantaneously and it creates a shock wave moving downstream, and a depression wave (rarefaction wave) propagating upstream. If the water depth ratio, h_d/h_u, is greater than 0.138, the flow throughout the channel remains subcritical (Stoker, 1958). For depth ratios smaller than 0.138, the flow downstream is supercritical while remaining subcritical upstream. For very small values of the depth ratio, the flow regime becomes strongly

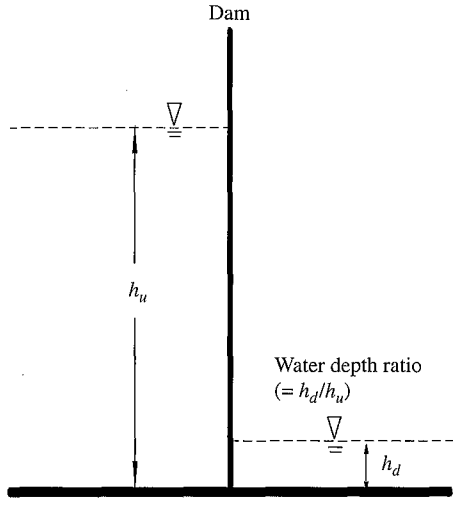

Fig. 1 The 1D dam-break problem

supercritical downstream and the shock wave can be difficult to capture. Therefore, the proposed schemes are tested to show their capability to solve severe dam-break flows.

Consider a horizontal and frictionless channel of 1000 m in length. A dam is located at the middle of the channel. The initial upstream water depth h_u is 10 m, and downstream water depths h_d are 0.05, and 0.001 m, respectively. Thus, two water depth ratios h_d/h_u of 0.005 and 0.0001 are considered for numerical tests. The Cournat number is set to be 0.8. For the comparisons of all first-order and second-order schemes, the space step Δx = 10 m. The simulation time is 25 s after the dam break. The exact solutions can be found in the literature (Stoker, 1958). Computations for these test cases were performed on a Pentium IV equipped with 256 megabyte RAM.

(i) Comparison of First-Order Upwind Schemes

Figures 2(a) and 2(b) show the simulated results from the three first-order upwind schemes with water depth ratios 0.005 and 0.0001, respectively. The comparison shows that all of them can predict the shock wave (wave-front) and the rarefaction wave without spurious oscillation. The simulated shock wave spreads over several grids and smears due to first-order accuracy of the schemes. The head and tail of the rarefaction wave (negative wave) are also too smearing. Thus, these first-order schemes produce numerical diffusion near corners, where the exact solution presents a discontinuity in a derivative. As shown in Fig. 2(a), the resolution of shock wave for the Roe scheme is a little better than that of the FVS or HLLE scheme in case of water depth ratio 0.005; while the FVS scheme has the highest resolution at the head corner of the rarefaction wave. In the case of the small water depth

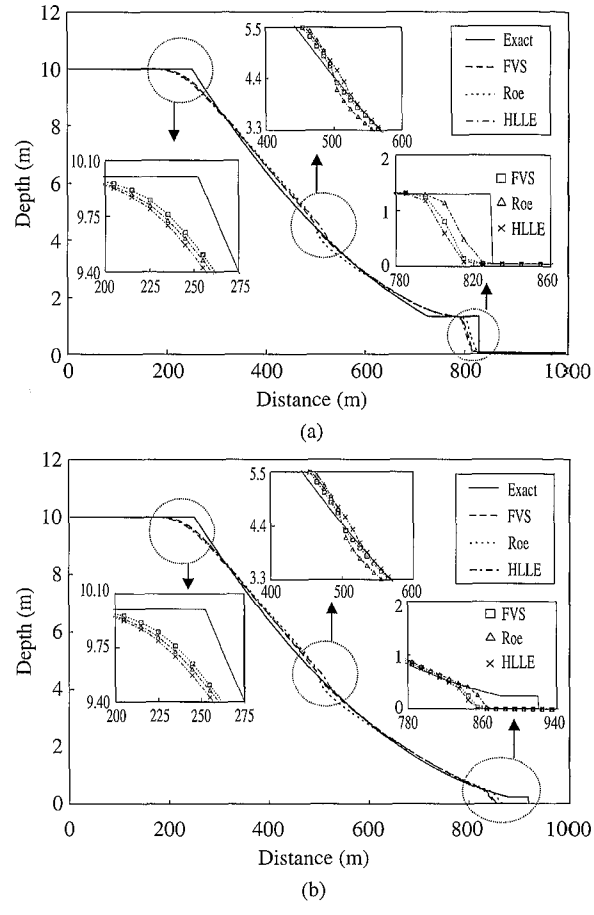

Fig. 2 Comparison of exact solutions with simulated depths using three first-order upwind schemes for the water depth ratios h_d/h_u of (a) 0.005 and (b) 0.0001

ratio of 0.0001, the Roe scheme also has the highest resolution of shock wave among those of the three schemes. The comparison in Fig. 2(b) indicates that if the water depth ratio decreases (i.e. strongly supercritical dam-break flow), the difference of numerical resolutions among these first-order schemes increases manifestly. From the simulated results presented in Fig. 2, it is found that the FVS scheme presents the best resolution in the rarefaction wave at the dam site, and it also produces better resolutions at the head corner of the rarefaction wave than those by the Roe and the HLLE schemes.

To evaluate the overall performance quantitatively in the whole flow regions, Table 1 summarizes the relative error L_2 norm and the computational time. To compare the relative error of the water depth in the simulation domain between simulated and exact solutions, the relative error L_2 norm is defined as (LeVeque, 1992):

$$L_2 = \sqrt{\frac{\sum (h_i^{\text{sim}} - h_i^{\text{exact}})^2}{\sum (h_i^{\text{exact}})^2}} \qquad (42)$$

Table 1 The L_2 norms and the CPU time for the idealized dam-break problem using three first-order upwind schemes

Depth ratio	L_2			CPU (s)		
	FVS	Roe	HLLE	FVS	Roe	HLLE
0.005	0.0339	0.0343	0.0374	0.046	0.078	0.055
0.0001	0.0211	0.0244	0.0266	0.062	0.105	0.075

Table 2 The L_2 norms and the CPU time for the idealized dam-break problem using three second-order flux-limited schemes

Depth ratio	L_2			CPU (s)		
	FVS-Sweby	Roe-Sweby	HLLE-Sweby	FVS-Sweby	Roe-Sweby	HLLE-Sweby
0.005	0.0202	0.0206	0.0212	0.087	0.151	0.105
0.0001	0.0118	0.0119	0.0135	0.111	0.189	0.143

where h_i^{sim} and h_i^{exact} are the simulated water depth and the exact solution at grid point i, respectively. Comparing the overall numerical accuracy, between the three tested schemes, the FVS scheme yields the smallest L_2 norm of water depth, whereas the HLLE gives the largest one. The overall numerical accuracy of the FVS scheme is better than those of the Roe and HLLE schemes. Moreover, the FVS scheme consumes, on the average, 78% and 16% less CPU time than the Roe scheme and the HLLE scheme, respectively. The CPU time consumed by the FVS scheme is the smallest. It implies that the FVS scheme has the best numerical performance.

(ii) Comparison of Second-Order TVD Schemes

The simulated results with water depth ratios 0.005 and 0.0001 by using FVS-Sweby, Roe-Sweby, and HLLE-Sweby schemes are shown in Fig. 3. Simulated results show that these second-order schemes result in better numerical resolutions. Compared with the simulated results by first-order scheme in Fig. 2, both the shock wave and rarefaction wave of dam-break flows are predicted obviously better by using these second-order TVD schemes. All schemes have similar resolution near both shock wave front and rarefaction wave, while the FVS-Sweby scheme produces the best fitting to the exact solution at the head of the rarefaction wave. The quantitative comparison of numerical performance from these second-order TVD schemes is listed in Table 2. The results indicate that the HLLE-Sweby scheme produces the largest relative error L_2 norm, and the Roe-Sweby scheme consumes the most computational time. Therefore, the FVS-Sweby scheme presents the best numerical performance among these three second-order schemes.

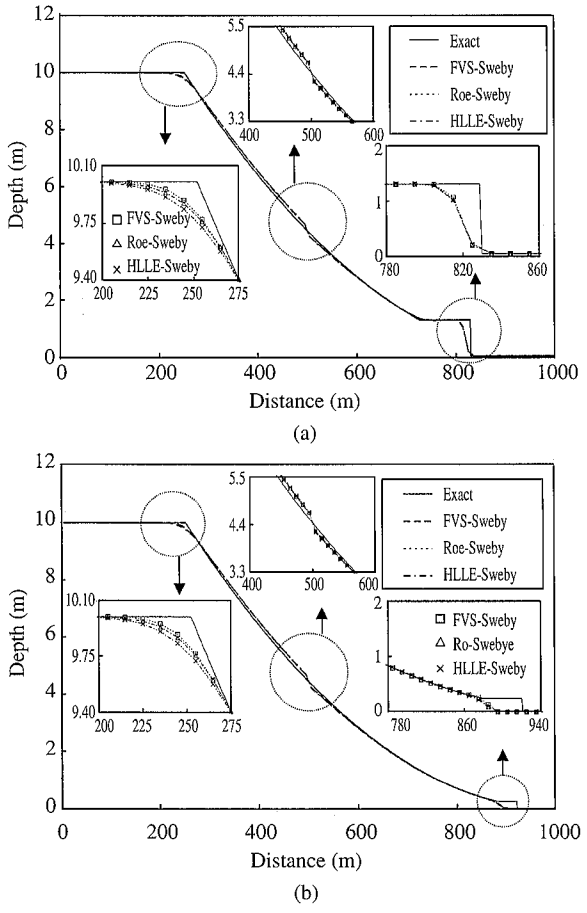

Fig. 3 Comparison of exact solutions with simulated depths using three second-order flux-limited schemes for the water depth ratios h_d/h_u of (a) 0.005 and (b) 0.0001

By employing FVS-DMH, Roe-DMH, and HLLE-DMH schemes for the idealized dam-break flows, the simulated results with water depth ratios

Table 3 The L_2 norms and the CPU time for the idealized dam-break problem using three second-order slope-limited schemes

Depth ratio	L_2			CPU (s)		
	FVS-DMH	Roe-DMH	HLLE-DMH	FVS-DMH	Roe-DMH	HLLE-DMH
0.005	0.0151	0.0157	0.0166	0.059	0.117	0.083
0.0001	0.0083	0.0084	0.0087	0.081	0.168	0.107

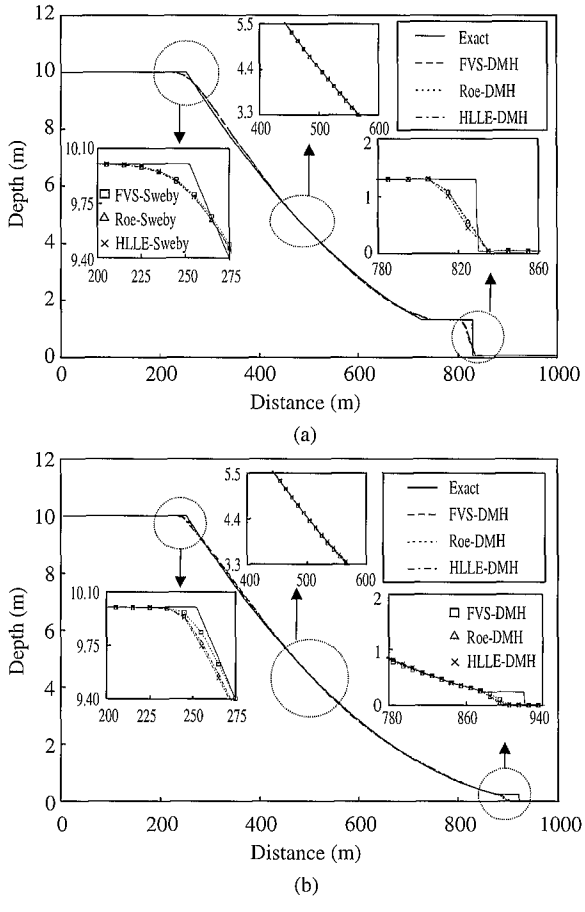

Fig. 4 Comparison of exact solutions with simulated depths using three second-order slope-limited schemes for the water depth ratios h_d/h_u of (a) 0.005 and (b) 0.0001

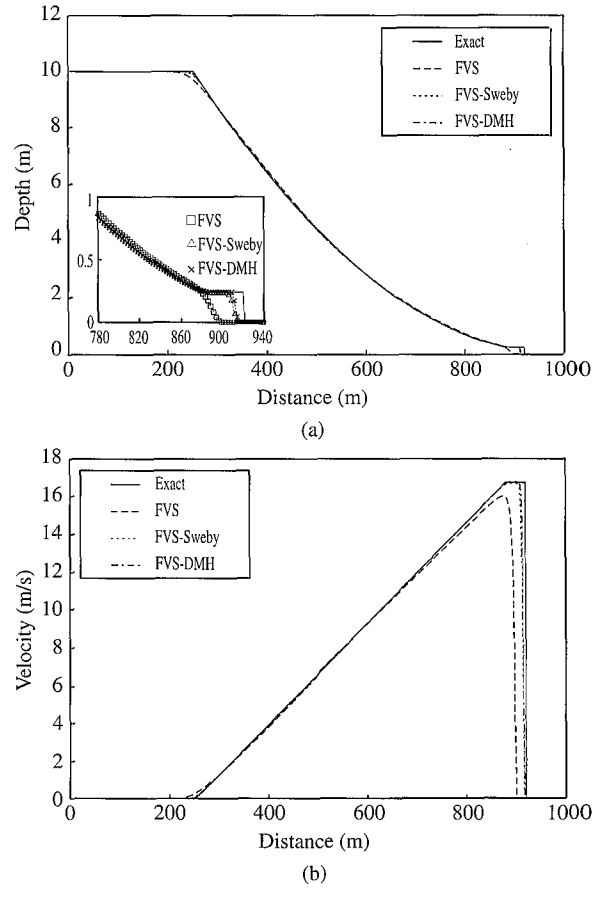

Fig. 5 Comparison of exact solutions with (a) simulated depths and (b) velocities using the FVS, FVS-Sweby and FVS-DMH schemes for a water depth ratio h_d/h_u of 0.0001

0.005 and 0.0001 are shown in Fig. 4. These results show that these second-order schemes can well predict the shock wave and rarefaction wave without spurious oscillations produced. All these second-order TVD schemes present rather good resolution for the supercritical dam-break flow downstream. A quantitative comparison of the above results is listed in Table 3. The CPU time consumed by the Roe-DMH scheme is more than the time consumed by FVS-DMH and HLLE-DMH schemes. The relative error L_2 norm of the HLLE-DMH scheme is the largest among the three schemes. Obviously, Table 3 shows that the FVS-DMH scheme produces the best numerical performance among the three schemes.

According to the above analyses of simulated results, it is apparent that the first-order upwind scheme with direct MUSCL-Hancock slope limiter approach has better numerical performance in terms of relative error L_2 norm and CPU computational time. On the other hand, it can be found that the FVS-based schemes have the best numerical performance among Roe-, HLLE- and FVS-based schemes. In addition, to demonstrate the difference of numerical performance, the first-order FVS and second-order FVS-Sweby and FVS-DMH schemes are used to simulate the supercritical dam-break flows with a water depth ratio h_d/h_u of 0.0001 using computational cells of 400. Fig. 5 presents the simulated water

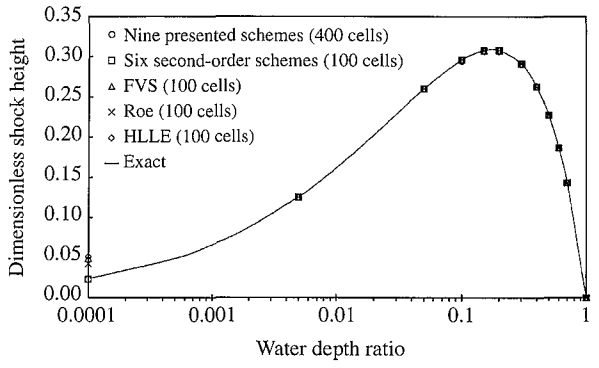

Fig. 6 Comparison of the exact solutions with the simulated dimensionless shock heights for the range of water depth ratios ($10^{-4} \le h_d/h_u \le 1$)

depths and velocities. It clearly shows that both second-order TVD (FVS-Sweby and FVS-DMH) schemes can obtain better resolution of shock wave as well as rarefaction wave than the first-order FVS scheme. In addition, the numerical resolution for the FVS-DMH scheme is better than that of the FVS-Sweby scheme. In the severe case of water depth ratio 0.0001, the dam-break flow regime becomes strongly supercritical downstream, and it seems difficult to capture the front of the shock wave well by TVD schemes. In the final analysis, the resolution of the shock front for the FVS-DMH scheme is better than that of the FVS-Sweby scheme.

Additionally, the comparison of the exact solutions with the simulated dimensionless shock height $(h_f - h_d)/h_u$ for a wide range of water depth ratios ($10^{-4} \le h_d/h_u \le 1$) is made and plotted in Fig. 6, where h_f is the water depth behind the shock. For the simulation condition with 100 computational cells, all presented schemes compare perfectly well with the exact solution except the three first-order FVS, Roe and HLLE schemes for the very small water depth ratio of 0.0001. The three presented first-order FVS, Roe and HLLE schemes predict higher wave fronts, whereas the presented six second-order schemes can simulate well. To improve prediction accuracy at the wave front, the cell grid is refined and computational cells increased up to 400. As shown in Fig. 6, the simulated dimensionless shock heights for all of the nine presented schemes with 400 computational cells match the exact solution quite well.

2. Dry Bed Dam-Break Flow

To demonstrate the presented schemes are capable of simulating flow over a dry bed, the dry bed dam-break problem is tested herein. Only the second-order FVS-DMH scheme is selected and tested. A channel with 2000 m in length is considered. The

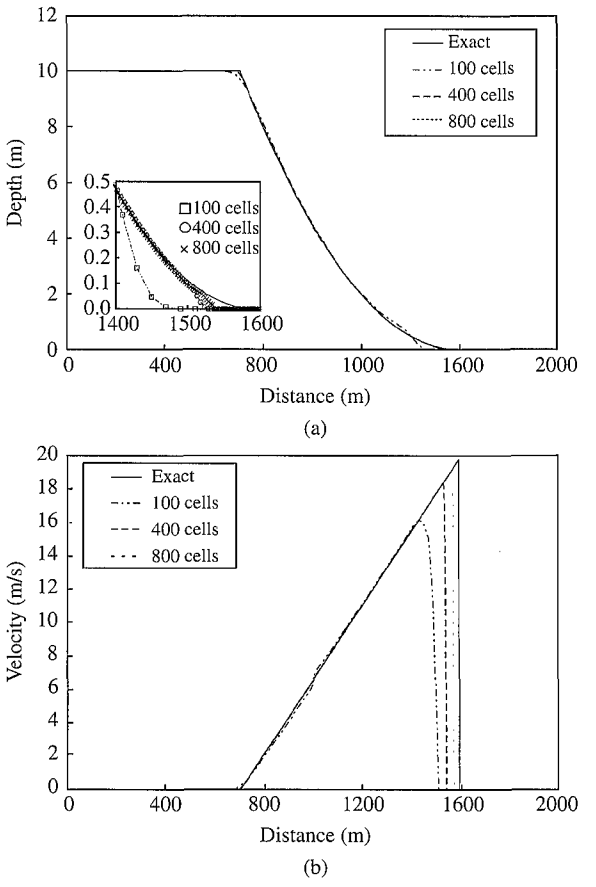

Fig. 7 The influence of the computational grid size on the simulated (a) water depths and (b) velocities using the FVS-DMH scheme for the dry bed dam-break problem

dam is located at 1000 m downstream of the channel inlet. The initial upstream and downstream water depths, h_u and h_d, are 10 m and 0 m, respectively. The CFL number is set to be 0.8. In this problem, there is a single rarefaction wave and no shock wave exists. Accordingly, an absolute zero depth in the dry bed can cause mathematical problems (Toro, 2001). To avoid this, an almost negligible water depth of 0.00001 m is assumed at the downstream channel bed of the dam. Three different computational cells of 100, 400 and 800 are considered. Comparison of exact solution with simulated depths and velocities at t = 30 s are presented in Figs. 7(a) and 7(b), respectively. The FVS-DMH scheme using 800 cells can predict the rarefaction wave quite well. From the close-up of the dry/wet fronts shown in Fig. 7(a), obviously the presented scheme using 800 cells captures the shock fronts in a steeper and less dissipative manner than those using 100 and 400 cells.

3. Dam-Break Experiment with Sudden Collapse

In order to demonstrate that the presented

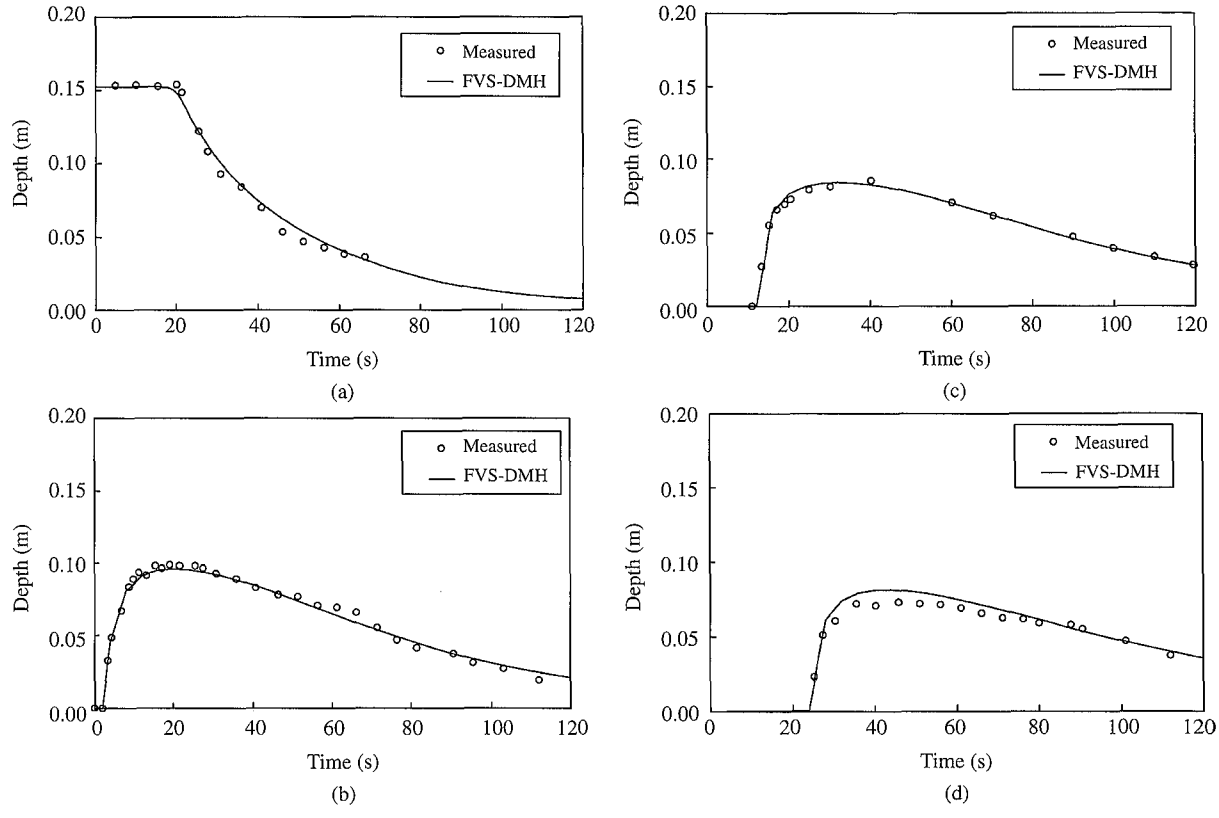

Fig. 8 Experimental and simulated results with sudden dam collapse at (a) x = 30.5 m, (b) x = 68.625 m, (c) x = 85.4 m, and (d) x = 106.625 m

numerical scheme is capable of describing real dam-break scenarios, the slope and friction components must be incorporated. In this section, only the second-order FVS-DMH scheme is selected and tested. The data of the dam-break experiment conducted by the Waterway Experiment Station (WES), US Corps of Engineers (1960) are adopted in this section.

The experiment was conducted in a 122 m long and 1.22 m wide rectangular channel with bottom slope of 0.005. The channel bed roughness is represented by a Manning coefficient of 0.009. Initially, the water depth on the upstream side of the dam is 0.305 m, and the downstream side of water depth is zero (dry bed). An absolute zero depth in the dry bed can cause mathematical problems (Toro, 2001). So, an almost negligible water depth of 0.00001 m is assumed at the downstream channel bed of the dam. The flow domain along the channel is discretized into 122 grids with the uniform grid spacing Δx =1.0 m. Figs. 8(a)-8(d) show the simulated results for WES experiments, in which the dam-break wave propagates downstream on a dry bed. The agreement between computed and measured water depth against time at various locations is good for the entire duration using the second-order FVS-DMH scheme. Fig. 9 shows the computed water-depth profile variations along the centerline of the flume at different times, where fairly good agreement

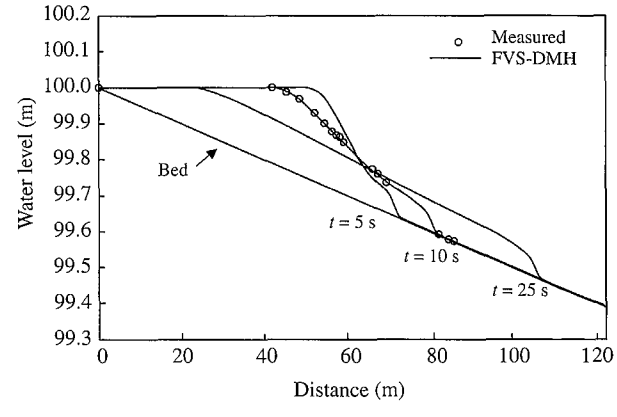

Fig. 9 The computed water levels at t = 5, 10, and 25 seconds and the measured water level at t = 10 seconds

has been obtained by use of the presented scheme. In conclusion, the application herein demonstrates the capability of the presented scheme to deal with channel friction, slope and dry bed condition.

V. CONCLUSIONS

In this paper, three robust and reliable first-order upwind schemes are presented and then extended to high-resolution TVD schemes based on two different

approaches, the Sweby flux limiter approach and the direct MUSCL-Hancock slope limiter approach. For idealized dam-break flow modeling, three first-order and six second-order TVD schemes are evaluated, and it is found that the FVS-DMH scheme is the best one. Then, the FVS-DMH scheme is applied to the dam-break experiment of WES. Important conclusions are as follows.

1. Among the three first-order upwind schemes, the FVS scheme uses less computational time and has the least L_2 error, while the Roe scheme spends the longest computational time, while it has a better resolution of shock wave front. Therefore, the presented FVS scheme may be useful for researchers who are seeking ways to make numerical codes run faster without the loss of accuracy.
2. Among three flux-limited schemes, the FVS-Sweby has the best numerical performance. In a like manner, the FVS-DMH also has the best numerical performance among three slope-limited schemes. Moreover, the FVS-Sweby and FVS-DMH schemes have the inherent properties of numerical performance from the first-order FVS scheme. Therefore, it is very important to use an accurate and efficient first-order scheme as a basis for higher-order extension.
3. Between the FVS-Sweby and FVS-DMH schemes, the FVS-DMH scheme is preferred because it has lower L_2 error and consumes less CPU time.
4. Refining cell grid can improve the accuracy of shock height prediction. The simulated dimensionless shock heights from all of the nine presented schemes with 400 computational cells match the exact solution quite well for the range of water depth ratios ($10^{-4} \le h_d/h_u \le 1$).
5. Application of the FVS-DMH scheme to the dam-break experiment case demonstrates the capability of the presented scheme to deal with channel friction, sloping bed and dry bed conditions.

NOMENCLATURE

$\boldsymbol{A}$	Jacobian matrix
C_n	Courant number
c	celerity of the gravity wave
$\boldsymbol{F}$	flux vectors in the x-direction
$\boldsymbol{F}_C$	convective flux vector
$\boldsymbol{F}^{(1)}_{i+1/2}$	first-order numerical flux
$\boldsymbol{F}^{(2)}_{i+1/2}$	second-order numerical flux
F_r	Froude number
g	gravity acceleration
$H^{(\Delta t)}$	homogeneous solution operator
h	water depth
h_d	initial water depths downstream of the dam
h_f	shock height
h_u	initial water depths upstream of the dam
h_i^{sim}	simulated water depth
h_i^{exact}	exact water depth
$\boldsymbol{I}$	identity matrix
L_2	relative error
n	time level
$O^{(\Delta t)}$	ordinary differential equation operator
$\boldsymbol{P}$	pressure vector
p	hydrostatic pressure
$\boldsymbol{R}^{(k)}$	eigenvectors
$\tilde{\boldsymbol{R}}^k$	average approximate eigenvectors
$\boldsymbol{S}$	vector of the source terms
s_0	slope of the channel bottom
s_f	friction slope
t	time
$\boldsymbol{U}$	vector of conserved variables
u	depth-averaged velocity
$\boldsymbol{W}$	flow variable vector
x	horizontal distance along a channel
Δx	grid spacing
Δt	time step
$\mathcal{F}_r^{\pm}$	split Froude number function
$\mathcal{P}^{\pm}$	split pressure function
$\overline{\Delta}_i$	slope limiter
ϕ	flux limiter
$\tilde{\alpha}_k$	average approximate wave strengths
$\tilde{\lambda}_k$	average approximate eigenvalues
λ_k	eigenvalues
τ	mesh ratio

REFERENCES

Alcrudo, F., Garcia-Navarro, P., and Saviron J. M., 1992, "Flux Difference Splitting for 1D Open Channel Flow Equations," *International Journal for Numerical Methods in Fluids*, Vol. 14, No. 9, pp. 1009-1018.

Chaudhry, M. F., 1993, *Open-Channel Flow*, Prentice-Hall, Englewood Cliffs, NJ, USA.

Delis, A. I., 2003, "Improved Application of the HLLE Riemann Solver for the Shallow Water Equations with Source Terms," *Communications in Numerical Methods in Engineering*, Vol. 19, No. 1, pp. 59-83.

Delis, A. I., and Skeels, C. P., 1998, "TVD Schemes for Open Channel Flow," *International Journal for Numerical Methods in Fluids*, Vol. 26, No. 7, pp. 791-809.

Delis, A. I., Skeels, C. P., and Ryrie, S. C., 2000, "Evaluation of Some Approximate Riemann Solvers for Transient Open Channel Flows," *Journal of Hydraulic Research*, Vol. 38, No. 3, pp. 217-231.

Einfeldt, B., 1988, "On Godunov-Type Methods for Gas Dynamics," *SIAM Journal on Numerical Analysis*, Vol. 25, No. 2, pp. 294-318.

Garcia-Navarro, P., Alcrudo, F., and Saviron, J. M.,

1992, "1D Open Channel Flow Simulation using TVD-MacCormack Scheme," *Journal of Hydraulic Engineering*, Vol. 118, No. 10, pp. 1359-1372.

Harten, A., 1983, "High Resolution Schemes for Hyperbolic Conservation Laws," *Journal of Computational Physics*, Vol. 49, No. 3, pp. 357-393.

Harten, A., and Hyman, J. M., 1983, "Self Adjusting Grid Methods for 1D Hyperbolic Conservation Laws," *Journal of Computational Physics*, Vol. 50, No. 2, pp. 235-269.

Harten, A., Lax, P. D., and van Leer, B., 1983, "On Upstream Differencing and Godunov-Type Schemes for Hyperbolic Conservation Laws," *SIAM Review*, Vol. 25, No. 1, pp. 35-61.

Hirsch, C., 1990, *Numerical Computation of Internal and External Flows*, 2nd ed., John Wiley & Sons, New York, USA.

Jha, A. K., Akiyama, J., and Ura, M., 1995, "First- and Second-order Flux Difference Splitting Schemes for Dam-Break Problem," *Journal of Hydraulic Engineering*, Vol. 121, No. 12, pp. 877-884.

LeVeque, R. J., 1992, *Numerical Methods for Conservational Laws*, Birkhauser Verlagl, Switzerland.

Lin, G. F., Lai, J. S., and Guo, W. D., 2003, "Finite-Volume Component-Wise TVD Schemes for 2D Shallow Water Equations," *Advances in Water Resources*, Vol. 26, No. 8, pp. 861-873.

Liou, M. S., and Steffen, C. J., 1993, "A New Flux Splitting Scheme," *Journal of Computational Physics*, Vol. 107, No. 1, pp. 23-39.

Roe, P. L., 1981, "Approximate Riemann Solvers, Parameter Vectors, and Difference Schemes," *Journal of Computational Physics*, Vol. 43, No. 2, pp. 357-372.

Stoker, J. J., 1958, *Water Waves: Mathematical Theory with Applications*, Wiley-Interscience, Singapore.

Strang, G., 1968, "On the Construction and Comparison of Finite Difference Schemes," *SIAM Journal on Numerical Analysis*, Vol. 5, No. 3, pp. 506-517.

Sweby, P. K., 1984, "High Resolution Schemes using Flux Limiters for Hyperbolic Conservation Laws," *SIAM Journal on Numerical Analysis*, Vol. 21, No. 5, pp. 995-1011.

Tan, W. Y., 1992, *Shallow Water Hydrodynamics*, Elsevier, New York, USA.

Toro, E. F., 1997, *Riemann Solvers and Numerical Methods for Fluid Dynamics*, Springer-Verlag, Berlin, Germany.

Toro, E. F., 2001, *Shock-Capturing Methods for Free-Surface Shallow Water Flows*, John Wiley & Sons, New York, USA.

Tseng, M. H., and Chu, C. R., 2000, "The Simulation of Dam-Break Flows by an Improved Predictor-Corrector TVD Scheme," *Advances in Water Resources*, Vol. 23, No. 6, pp. 637-643.

United States Army Corps of Engineers, Waterways Experiment Station (WES), 1960, "Flood Resulting from Suddenly Breached Dams," *Miscellaneous Paper, No. 2-374*, Vicksburg, MI, USA.

van Leer, B., 1979, "Towards the Ultimate Conservation Difference Scheme V, A Second-order Sequel to Godunov's Method," *Journal of Computational Physics*, Vol. 32, No. 3, pp. 101-136.

van Leer, B., 1984, "On the Relation Between the Upwind-Differencing Schemes of Godunov, Engquist-Osher and Roe," *SIAM Journal of Scientific and Statistical Computing*, Vol. 5, No. 1, pp. 1-20.

Yang, J. Y., Chang S. H., and Hsu, C. A., 1993, "Computations of Free Surface Flows, Part 1. One-Dimensional Dam-Break Flow," *Journal of Hydraulic Research*, Vol. 31, No. 1, pp. 19-34.

Yee, H. C., 1987, "Construction of Explicit and Implicit Symmetric TVD Schemes and Their Applications," *Journal of Computational Physics*, Vol. 68, No. 1, pp. 151-179.

Zhao, D. H., Shen, H. W., Lai, J. S., and Tabios, G. Q., 1996, "Approximate Riemann Solvers in FVM for 2D Hydraulic Shock Wave Modeling," *Journal of Hydraulic Engineering*, Vol. 122, No. 12, pp. 692-702.

Zoppou, C., and Roberts, S., 2003, "Explicit Schemes for Dam-Break Simulations," *Journal of Hydraulic Engineering*, Vol. 129, No. 1, pp. 11-34.

Manuscript Received: Dec. 08, 2003
Revision Received: Jan. 28, 2005
and Accepted: Mar. 01, 2005